RSC Advances

ROYAL SOCIETY OF CHEMISTRY

www.rsc.org/advances

Journal Name

ARTICLE

Reactive porous composites for chromium(VI) reduction applications based on Fe/carbon obtained from post-consumer PET and iron oxide.

Received 00th January 20xx,
Accepted 00th January 20xx

DOI: 10.1039/x0xx00000x

www.rsc.org/

Lílian A. Carvalho,[a] José D. Ardisson,[b] Rochel M. Lago,[a] Maria D. Vargas[c,*] and Maria H. Araujo[a,*]

By using post-consumer PET waste and iron oxide (Fe_2O_3) novel porous magnetic Fe/carbon composites for environmental applications have been obtained by a very simple process. XRD, Mössbauer, TG/MS, SEM, BET and Raman analyses have indicated that molten PET containing dispersed Fe_2O_3 particles decomposes in the 500-1000°C range to produce a carbon matrix with developed micro and mesoporosities and surface areas of 136-260 m^2g^{-1}, with simultaneous reduction of Fe^{3+} to iron phases whose composition depended on the decomposition temperature: i) reactive Fe^{2+} phases, FeOOH, Fe_3O_4 (magnetite) and FeO (wüstite) for the composites obtained at 500-600 °C and ii) Fe^0 and Fe_3C for those obtained at higher temperatures. Investigation of these composites for the reduction of aqueous chromium(VI) showed high activities for the materials obtained at 500 and 600 °C, which is discussed in terms of the phase composition and presence of carbon surface oxygen groups for the adsorption of Cr^{3+}.

Keywords: PET waste, Fe reduced phases, porous carbon, chromium(VI) removal

1 Introduction

Reactive composites based on carbon and reduced iron species have been investigated for different environmental applications, such as reduction of organochloro compounds,[1-3] chromium(VI),[4-18] nitroaromatics,[19] dyes,[20] pesticides,[21] nitrate/nitrite[22] and oxidations *via* the Fenton reaction.[23-25] Some of these composites showed very good reactivities and the possibility of regeneration after use and deactivation, *i.e.* the oxidized iron species in the composite can be reduced and regenerated by simple thermal treatment.[4] Different approaches have been used for the production of iron reduced reactive species with different reductants, such as activated carbon,[4] tar pitch[5,9] and H_2.[26,27]

In this work we report the preparation of a reactive Fe/carbon porous composite by a very simple process using post-consumer polyethylene terephthalate (PET) waste and iron oxide (Fe_2O_3). A schematic representation of the preparation route for the Fe/carbon porous composites is shown in Fig. 1.

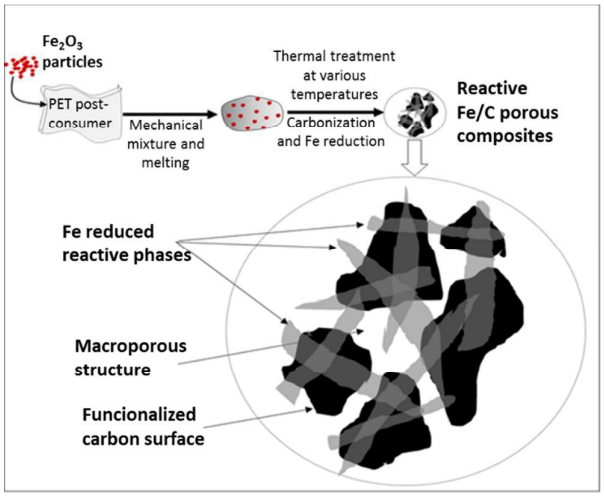

Fig. 1 Schematic representation of the preparation of the Fe/C_{PET} composites.

Different applications for post-consumer PET have been proposed, including the production of fibers,[28] polymer blends,[29,30] cationic exchange resins[31] and building.[32,33] The carbonization of PET has also been previously described,[34-36] however the use of PET in the process depicted in Fig. 1 is new and contemplates several important features. PET is a hydrophilic polymer, which can interact and efficiently disperse iron oxide particles. Thermal decomposition of PET produces small molecules, such as CO, volatile organics and a

[a] *Departamento de Química, Universidade Federal de Minas Gerais, Belo Horizonte-MG, CEP 35400-000, Brazil.*
[b] *Laboratório de Física Aplicada, Centro de Desenvolvimento da Tecnologia Nuclear, Belo Horizonte-MG, CEP 30123-970, Brazil.*
[c] *Instituto de Química, Universidade Federal Fluminense, Campus do Valonguinho - Centro - Niterói - RJ, CEP 24020-141, Brazil.*
Electronic Supplementary Information (ESI) available: [details of any supplementary information available should be included here]. See DOI: 10.1039/x0xx00000x

carbon matrix, which should act as reducing agents for iron oxide, yielding iron reduced species. Furthermore, the reaction of iron oxide with the PET carbon matrix should have an activation effect in the formation of a porous structure with significant surface area. The high oxygen content in PET can potentially generate oxygen functional groups on the formed carbon surface, such as –COOH (carboxylic) and –OH (phenolic), which can play several important roles in adsorption processes. Another interesting potential feature of this process is that the iron oxide used can be obtained from different wastes and natural materials.[37]

Herein, the preparation and characterization of different Fe/C_{PET} composites, and their use for the reduction of hazardous aqueous and soil contaminant chromium(VI) is described. Hexavalent chromium in the environment comes from different industrial activities, *e.g.* electroplating, leather tanning, pulp production, ore and petroleum refining processes.[38] Chromium(VI) compounds are contaminants of special concern due to a combination of several factors, including high mobility of its oxyanions, *e.g.* CrO_4^{2-} and $Cr_2O_7^{2-}$ in water and soils,[39] its oxidation potential and carcinogenic/mutagenic activities.[40] Efficient technologies for the removal of hazardous chromium(VI) contaminants are, therefore, of considerable interest.

2 Experimental

2.1 Chemicals

$Fe(NO_3)_3.9H_2O$ (Vetec), sulfuric acid (Synth), 1,5-diphenylcarbazide (Vetec) and K_2CrO_4 (Synth) were used without further purification. Post-consumer PET from colorless beverage bottles was used for the preparation of the carbon-coated reactive composites.

2.2 Preparation of hematite and composites

Hematite was obtained by slowly heating $Fe(NO_3)_3.9H_2O$ (20 g) in a beaker from 30 to 150 ^oC until it dried and became a red powder. This red powder was transferred to a tubular furnace (Lindberb Blue M) and heated from 30 to 450 ^oC (at 15 °C/min, in air), and kept at this temperature for 4 h, after which time it was allowed to cool down to room temperature inside the furnace. The Fe/C_{PET} composites were prepared by mixing 8 g of molten PET (at 270 ^oC) with 2 g of the powdered hematite. The red Fe_2O_3/PET composite was then cooled down and broken into small pieces (*ca.* 2 mm). Portions of this material (5 g) were heated in a tubular furnace (10 °C/min, under N_2 atmosphere) to 500, 600, 700, 800, 900 or 1000 °C and kept at the given temperature for 30 min, yielding black samples of Fe_{500}/C_{PET}, Fe_{600}/C_{PET}, Fe_{700}/C_{PET}, Fe_{800}/C_{PET}, Fe_{900}/C_{PET} and Fe_{1000}/C_{PET}, respectively, that were kept in a desiccator in the air.

2.3 Characterization

The X-ray diffraction patterns were obtained on a Rigaku, Geigerflex model diffractometer using Ni filtered Cu-Kα radiation (30 kV, 30 mA, λ = 1.54184 Å) with an angle of 2θ which was varied from 4 to 60 degrees at a rate of 2^o/min. Mössbauer spectroscopy was carried out using a spectrometer CMTE MA250 model, with a source of cobalt-57 in rhodium matrix (^{57}Co/Rh) and α-Fe as reference. The spectra obtained were fitted using the Normos-90 program. Measurements of nitrogen (99.999%) adsorption/desorption at 77 K were carried out using volumetric adsorption equipment (Autosorb 1 Quantachrome). Prior to such measurements the samples were degassed at 150 °C for 12 h until the residual pressure was less than 0.5 Pa. Brunauer–Emmett–Teller (BET) and Barrett–Joyner–Halenda (BJH) equations were used to calculate surface area and pore size distribution, respectively. Scanning electron microscopy (SEM) images were taken with the FEI Quanta 200 FEG at an operating voltage of 2–20 kV. The samples were prepared by deposition on a carbon tape. To observe genuine pore structures on the external surface, the samples were observed without metal coating. Raman spectroscopy were performed at a Bruker Senterra model, using a helium neon laser at 633 nm line, power of 2 mW, as excitation source and a CCD detector. This spectrometer has an OLYMOUS BX51 optical microscope, 20x magnification, with a typical resolution of 1 cm^{-1} for 5 accumulation of 5 s. The FTIR was performed using a Perkin-Elmer Spectrum GX FT-IR spectrometer with KBr pellets, with analysis between 4000-400 cm^{-1}, resolution of 4 cm^{-1} and 64 accumulations for sample. The KBr pellets were prepared using a Perkin-Elmer press (7 tons), diluting the sample of interest in KBr in the ratio of 1:100. UV-Vis absorption spectra were used to determine chromium(VI) concentration with a Shimadzu UV 2550 spectrophotometer interfaced with a microcomputer. The quartz cuvette used has 1 cm optical path and analyzes were recorded between 190 and 800 nm. CHN elemental analysis were obtained using a Perkin-Elmer 2400-CHN equipment and used to carbon and hydrogen dosage. Flame atomic absorption spectrometry (FAAS) was used to determine the iron dosage in the samples using a Varian AA240FS spectrometer model, with air-acetilene mixture flame. Thermogravimetric analyses coupled to mass spectrometry were performed in a thermobalance NETZSCH model STA 449 F3, coupled to a mass spectrometer NETZSCH Aëolos model QMS 403C. The mass spectrometer is equipped with a source of ionization by electron impact and a quadrupole mass analyzer. For the analysis *ca.* 20 mg of sample were heated in an argon flow of 20 ml min^{-1} in the temperature range between 40 and 900 ˚C and a heating rate of 5 °C min^{-1}. The operating range of the mass analyzer is one 1-100 u.a.m.

2.4 Chromium(VI) reduction studies

Chromium(VI) reduction was performed using 10 mL of a K_2CrO_4 solution containing 50 mg L^{-1} of chromium (initial pH *ca.* 4.0) with 10 mg of the composites. The mixtures were shaken for 24 h at 200 rpm and 25 ± 2 °C (using an Ovan Orbital Maxi). After which time the composites were magnetically separated and an aliquot of 0.1 mL was collected. The concentration of unreacted chromium(VI)

was determined by the DPC method,[41] which involved addition of 1,5-diphenylcarbazide (5 g L^{-1} in acetone) at pH 1.0 (H_2SO_4) and spectrophotometric determination of the concentration of the red complex at 542 nm.

3 Results and discussion

Hematite (Fe_2O_3) prepared by thermal treatment of iron(III) nitrate at 450°C was fully characterized by XRD, Mössbauer and Raman spectroscopy (Fig. S1 in ESI). The XRD data suggests crystallite average size of *ca.* 31 nm forming micro spherical particles, which agglomerate to form large aggregates, as confirmed by the SEM images (Fig. 2). The hematite was mixed with PET, ground and melted at 270°C to produce the Fe_2O_3/PET precursor. SEM images suggest good dispersion of the Fe_2O_3 in the PET matrix with the presence of some agglomerates.

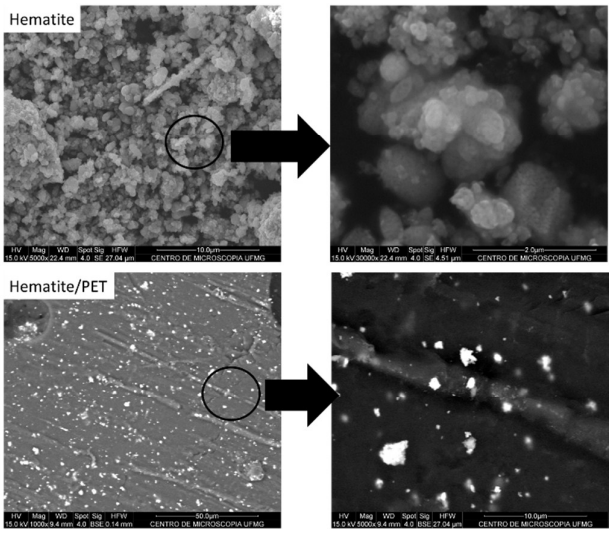

Fig. 2 SEM images of the prepared hematite and of the Fe_2O_3/PET precursor.

The Fe_2O_3/PET precursor was thermally treated at 500-1000°C under N_2 atmosphere and the products, named hereafter as Fe_{500}/C_{PET}, Fe_{600}/C_{PET}, Fe_{700}/C_{PET}, Fe_{800}/C_{PET}, Fe_{900}/C_{PET} and Fe_{1000}/C_{PET} accordingly. The Mössbauer spectra of the different Fe/C_{PET} samples are shown in Fig. 3 and the hyperfine parameters are presented in Table S1 (ESI). The Fe_{500}/C_{PET} and Fe_{600}/C_{PET} composites showed similar phase compositions with the presence of Fe_2O_3 (15-18 %), FeOOH (16-17%), magnetite (Fe_3O_4 53-57%) and wüstite (FeO 9-15%). The spectra of Fe_{700}/C_{PET}, Fe_{800}/C_{PET}, Fe_{900}/C_{PET} and Fe_{1000}/C_{PET} composites, however, only evidenced the presence of metallic iron (30-80%) and iron-carbon alloys Fe_3C (20-70%). Fig. 4 summarizes the iron phase compositions for the different composites.

The XRD patterns (Fig. 5) confirmed the Mössbauer spectroscopy results. The diffractograms of the samples Fe_{500}/C_{PET} and Fe_{600}/C_{PET} showed peaks associated to magnetite (Fe_3O_4 - PDF 19-629) and wüstite (FeO - PDF 2-1180), whereas those of samples Fe_{700}/C_{PET}, Fe_{800}/C_{PET}, Fe_{900}/C_{PET} and Fe_{1000}/C_{PET} showed peaks due to metallic iron (Fe - PDF 6-696), iron carbide (Fe_3C - PDF 23-1113) and graphitic carbon (C - PDF 3-401).

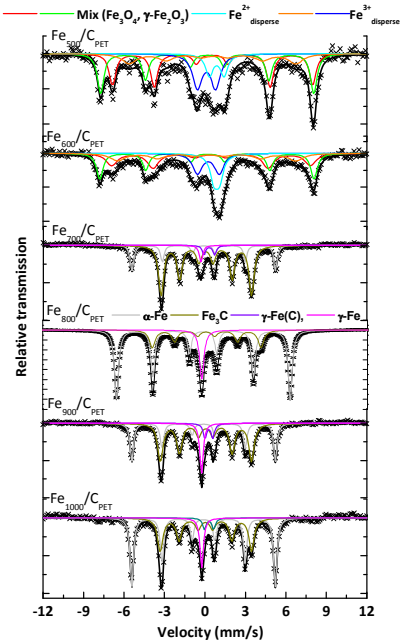

Fig. 3 Mössbauer spectra of Fe/C_{PET} samples.

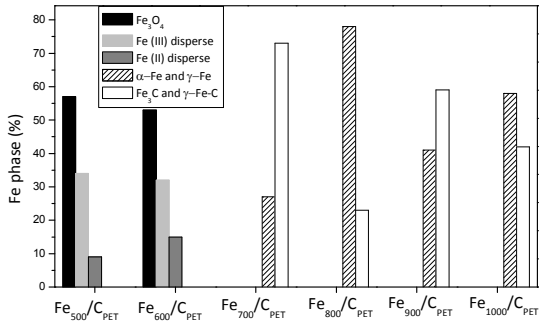

Fig. 4 Iron phase compositions for the Fe/C_{PET} composites according to Mössbauer spectroscopy.

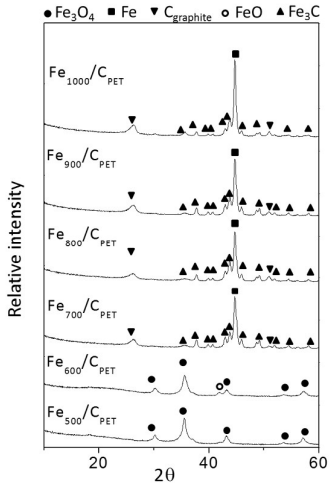

Fig. 5 XDR patterns for the produced composites.

The thermogravimetric curves obtained for PET and Fe_2O_3/PET samples in N_2 atmosphere are shown in Fig. 6.

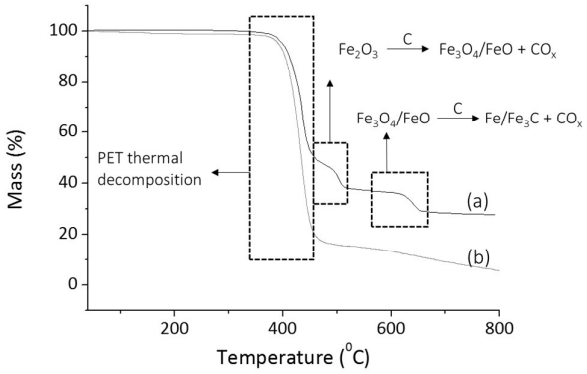

Fig. 6 TG curves for (a) the precursor (a mixture of 20% Fe_2O_3 in PET) and (b) pure PET, under inert atmosphere.

The TG curve obtained for the pure PET sample showed weight loss of *ca.* 80% around 430 °C, due to the decomposition and carbonization of the polymer, which produces mainly CO, CO_2, H_2O and other volatile organic molecules.[42] As the temperature increases, a gradual weight loss is observed leaving only 5% of carbon at 800°C. The TG curve for the PET mixed with 20% Fe_2O_3 (precursor) also shows initial weight loss around 440°C (about 60%). With the temperature increase two other processes are clearly observed around 500 and 650°C. These results are in accordance with the Mössbauer and XRD data, which evidenced different phase compositions for the samples obtained below and above 600°C. Thus the first process at about 500 °C is most likely related to the reductions of Fe_2O_3 to Fe_3O_4 and FeO by CO and organic volatile molecules from the decomposition of PET (Eq. 1 and 2):

$$Fe_2O_3 + \text{volatiles} \xrightarrow{400\text{-}500\ ^\circ C} Fe_3O_4/FeO \qquad \text{Eq.1}$$

$$Fe_3O_4 + C_{PET} \xrightarrow{400\text{-}500\ ^\circ C} FeO + CO_x \qquad \text{Eq.2}$$

The significant weight loss observed at 650°C is probably due to the further reduction reactions of the iron oxides to yield metallic iron, which combines further with carbon to produce iron carbides (Eq. 3 and 4). All these reactions have been previously observed.[5]

$$Fe_3O_4 + C_{PET} \xrightarrow{650\ ^\circ C} 3Fe^0 + CO_x \qquad \text{Eq.3}$$

$$Fe^0 + C \xrightarrow{650\ ^\circ C} Fe_3C \qquad \text{Eq.4}$$

It is interesting to observe that the iron oxide induces carbonization of the polymer, since pure PET decomposes to produce only 5% carbon whereas PET/Fe_2O_3 led to the formation of 29% of material. TG analyses in air were carried out to determine the carbon and iron contents in the Fe_x/C_{PET} samples. The results, gathered in Table 1, indicate that the composites obtained at 500 and 600 °C have the same carbon and iron compositions and considering the Mössbauer data (Fig. 3 and Table S1 in ESI) are in fact the same material. The carbon and iron content by TG were calculated considering that the high temperature and the oxidant atmosphere favor oxidation of carbon to CO_2 and iron compounds to iron (III) oxide - Fe_2O_3.

Table 1 Carbon and iron contents in the composites, determined by TGA[a] and FAAS[b].

Material	%C[a]	%Fe[a]	%Fe[b]
Fe_{1000}/C_{PET}	31	48	46
Fe_{900}/C_{PET}	33	45	41
Fe_{800}/C_{PET}	33	45	50
Fe_{700}/C_{PET}	33	46	48
Fe_{600}/C_{PET}	46	35	39
Fe_{500}/C_{PET}	46	34	40

The Raman spectra of the composites (Fig. 7) exhibited the typical D and G bands, which are characteristic of less organized and organized carbons, respectively.[43] The increase of the area of the G band compared to the D band with the increase in the temperature of composite treatment indicates formation of more organized carbon. Also, the presence of the G´ band at 2750 cm^{-1} suggests formation of graphitic structures.[43]

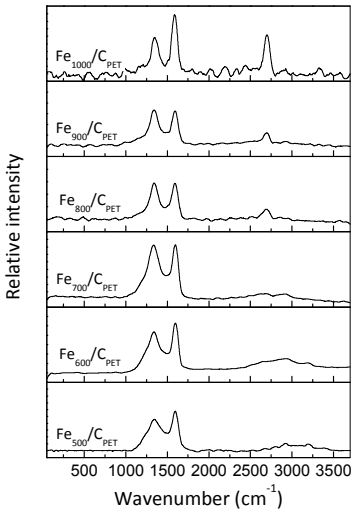

Fig. 7 Raman spectra of the Fe/C_{PET} composites.

TG-MS analyses of the Fe/C_{PET} samples confirm the presence of oxygenated groups on the carbon surface of Fe_{500}/C_{PET} and Fe_{600}/C_{PET}. In the TG-MS of Fe_{600}/C_{PET} (Fig. 8) the peak observed at *m/z* = 44, at 250-400˚C, is likely due to CO_2 formed from the decomposition of carboxylic groups,[44] and CO_2 evolution around 600˚C is probably due to lactone-type groups.[44] Semiquantitative

considerations using potassium oxalate for the calibration of the TG-MS, suggest the presence of 0.1 $mmol_{COOH}/g_{(Fe600/CPET)}$ and 0.2 $mmol_{COOH}/g_{(Fe500/CPET)}$. The other materials presented much lower concentration of surface oxygenated groups (see supplementary information Fig S2). The scanning electron microscopies of the composites obtained at different temperatures (Fig. 9) indicate that the spherical Fe_2O_3 aggregate particles well dispersed throughout the PET matrix (Fig. 2 Hematite/PET) are converted to needle-like shaped rectangular particles (pointed at Fig.9a and Fig.9b). EDS mapping (Fig. S3 in ESI) suggests that the Fe is homogeneously distributed throughout the particles. The needle-like rectangular particles seem to be wrapped by a material likely related to carbon. These agglomerated particles present a developed large porous structure in the space formed in between the needle crystals and the carbon. Similar textures have been observed for the composites obtained at 500-900°C. On the other hand, at 1000°C a significant sintering seems to take place to form more compacted particles.

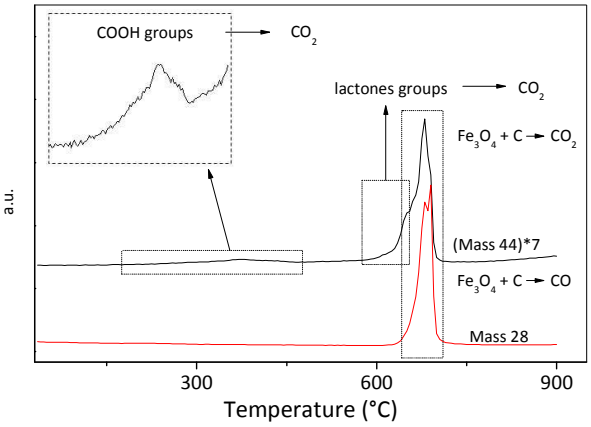

Fig 8 TG-MS profile of *m/z* 28 (CO) and 44 (CO_2) during thermal treatment of the composite Fe_{600}/C_{PET}

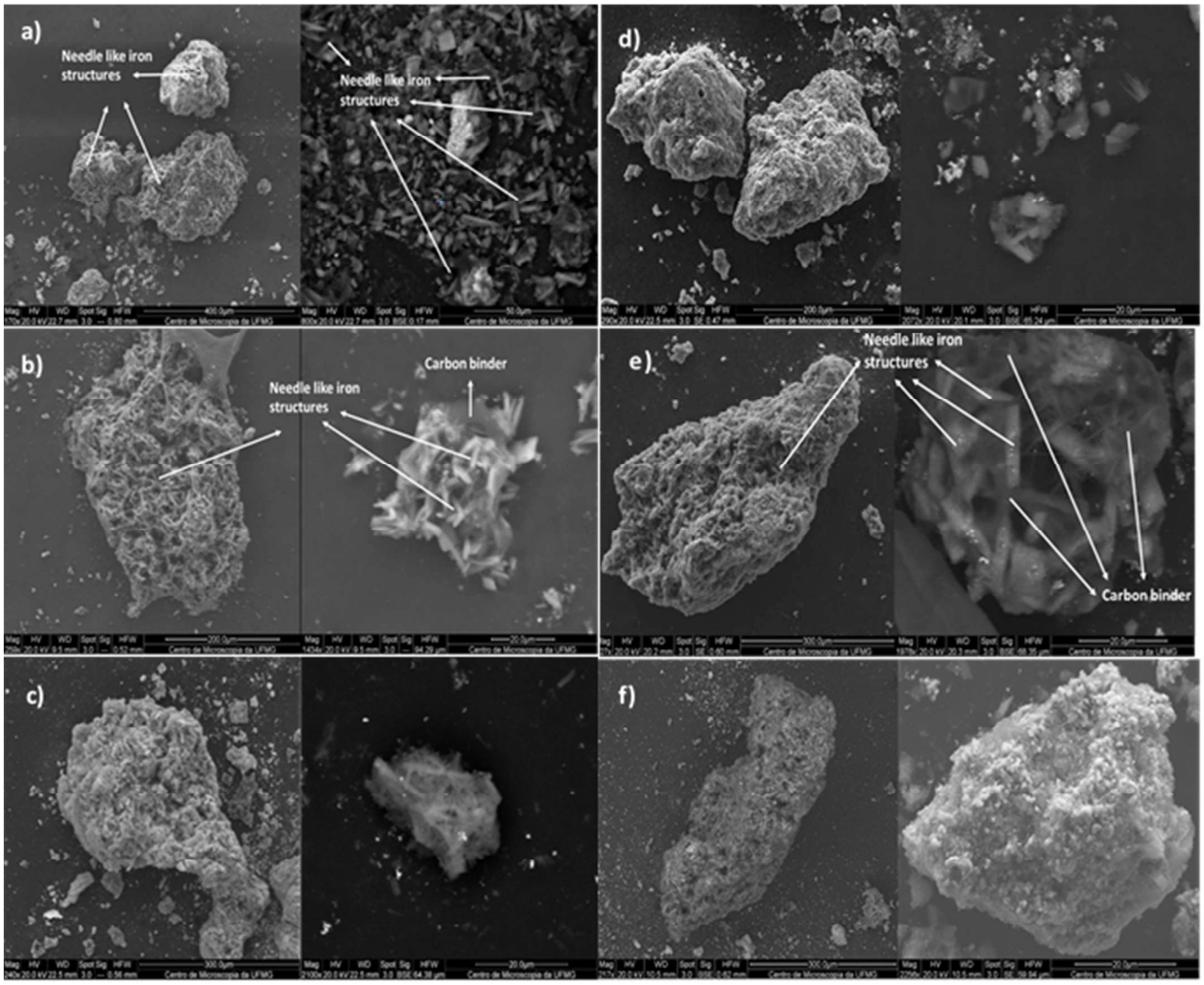

Fig. 9 SEM microphotographs for the different Fe/C_{PET} composite: Fe_{500}/C_{PET} (a), Fe_{600}/C_{PET} (b), Fe_{700}/C_{PET} (c), Fe_{800}/C_{PET} (d), Fe_{900}/C_{PET} (e) and Fe_{1000}/C_{PET} (f).

BET nitrogen adsorption/desorption measurements (Fig. S4 in ESI) showed no significant surface area for the Fe_2O_3/PET precursor. Upon treatment at 500 °C, however, the surface area increased to 262 m^2g^{-1} with the formation of pores with average diameter of 4 nm. As the treatment temperature increased to 600, 800 and 1000 °C the surface area decreased to 230, 195 and 136 m^2/g, respectively. It is interesting to observe that the carbon material obtained from the carbonization of pure PET (without Fe_2O_3), at 600 °C, did not show any significant surface area or porosity. These results suggest that the Fe_2O_3 particles have an activation effect during the carbonization of PET and contribute to increase the composite surface area. The adsorption and desorption isotherms and the pore diameter distribution of the composites are shown in the supplementary information (Fig. S4-S5 in ESI). The Fe_{500}/C_{PET} and Fe_{600}/C_{PET} samples showed mainly microporosity, whereas the Fe_{800}/C_{PET} and Fe_{1000}/C_{PET} samples showed a significant presence of mesopores.

3.1 Chromium(VI) reduction

Metallic iron and magnetite phases are known reducing agents for aqueous chromium(VI).[9] Considering the presence of low oxidation state iron compounds on the surface of the Fe/C_{PET} composites, these materials were tested as chromium(VI) reductants, and the results are gathered in Fig. 10. The experiments were carried out with 10 mg of each reducing material (Fe/C_{PET} composites) and 30 mL of a K_2CrO_4 solution containing 50 mg L^{-1} of chromium(VI), *i.e.* 150 mg of chromium/g of the reducing material, at 25 °C, for 24 hours.

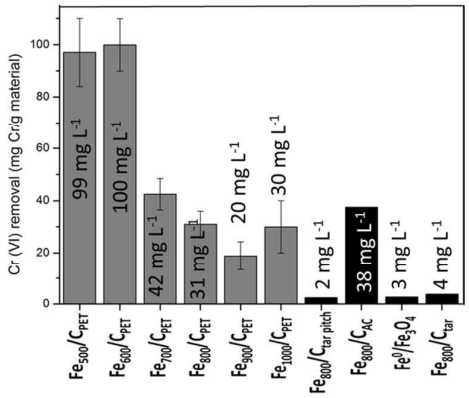

Fig. 10 Total chromium removal from a Cr(VI) aqueous solution during reduction tests in the presence of the Fe/C_{PET} composites and other known reducing materials.

The results indicate that composites Fe_{600}/C_{PET} and Fe_{500}/C_{PET} are the most efficient, reducing *ca.* 100 mg_{Cr}^{6+} g^{-1}, *i.e.* around 70% of the chromium present in solution after 24 h. As the composite treatment temperature increased to 700-1000 °C chromium(VI) reduction significantly decreased to 20-40 mg_{Cr}^{6+} g^{-1} after the same period of time. The activities of the following analogous chromium(VI) reducing materials previously described in the literature were also investigated under the same conditions for comparison: $Fe_{800}/C_{tarpitch}$ (obtained from Fe_2O_3 tar pitch at 800°C),[9] Fe_{800}/C_{AC} (obtained from Fe^{3+} impregnated on activated carbon 800 m^2 g^{-1} at 800°C),[4] Fe_{800}/C_{tar} (obtained from Fe_2O_3 tar at 800°C)[5] and a ground Fe^o/Fe_3O_4 mixture.[6] As shown in Fig. 10 the Fe_{500}/C_{PET} and Fe_{600}/C_{PET} composites exhibited much higher activity compared to all the other materials. Even the less active composites Fe_{700}/C_{PET}, Fe_{800}/C_{PET}, Fe_{900}/C_{PET} and Fe_{1000}/C_{PET} were more active than the materials described in the literature and similar to the high surface area Fe_{800}/C_{AC}.[4] The reasons for the higher chromium(VI) removal efficiency of the Fe_{500}/C_{PET} and Fe_{600}/C_{PET} composites are most probably related to the Fe composition in each composite and possibly also to their surface characteristics, *e.g.* area and reactivity. At 500 and 600 °C, Fe is present as different reducing phases, *i.e.* FeO, Fe_3O_4 and Fe^{2+}, all of which are well known chromium(VI) reductants.[5,9,20] At 700°C and higher temperatures all these phases are reduced to produce Fe^o and Fe_3C according to Mössbauer and XRD data. The carbide phase is very stable and does not seem to react with chromium(VI) under the employed reaction conditions. Furthermore, the Fe^o phase present in the composites produced above 700 °C is likely passivated by carbon and not efficient to reduce the aqueous Cr(VI) species. Therefore, the results obtained for the materials treated above 700 °C are very similar (considering the experimental error bar, Fig 10). It can also be considered that PET, a highly oxygenated polymer, during thermal decomposition at 500 and 600°C produces carboxylic surface groups, as observed by TG-MS analyses, which has been observed before.[45] These surface carboxylic groups can play an important role in chromium (Cr^{3+}) removal by adsorption. A simplified process showing Cr^{6+} reduction to the cation Cr^{3+} on the carbon surface is shown in Fig. 11.

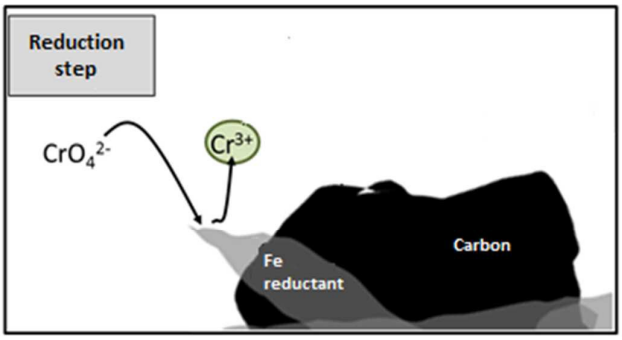

Fig. 11 Simplified process showing Cr^{6+} reduction to Cr^{3+} and adsorption on the carbon surface.

Another interesting feature of these reactive composites is the facile dispersion in aqueous medium and separation by magnetic processes. The Fe/C_{PET} composites can be dispersed in water, likely due to presence of very hydrophilic oxygen surface groups formed during the PET decomposition. As the composites are strongly magnetic, the dispersed powder can be easily attracted and removed by a simple magnet (see Fig. S6 in ESI). Moreover, preliminary experiments showed that the composites can be regenerated and reused several times by treatment at 800 °C for 1h, according to previous published results.[5]

4 Conclusion

Reactive magnetic porous carbon containing exposed iron reducing species can be prepared from PET waste and iron oxides by a very simple and low cost process. The magnetic porous carbon produced at 500 and 600°C showed the presence of different Fe^{2+} phases, which were very active for chromium(VI) removal, superior to other materials described in the literature. These results illustrate a new and exciting possibility to use different wastes to produce versatile materials for different environmental applications.

Acknowledgements

The authors acknowledge the financial support provided from FAPEMIG, CNPq, CAPES and Centro de Microscopia/UFMG.

Notes and references

1 W. F. Chen, L. Pan, L. F. Chen, Q. Wang and C. C. Yan, Dechlorination of hexachlorobenzene by nano zero-valent iron/activated carbon composite: iron loading, kinetics and pathway, *RSC Adv.*, 2014, 4, 46689-46696.

2 H. H. Tseng, J. G. Su and C. J. Liang, Synthesis of granular activated carbon/zero valent iron composites for simultaneous adsorption/dechlorination of trichloroethylene, *J. Hazard. Mater.*, 2011, 192, 500-506.

3 Z. Wang, P. a. Peng and W. Huang, Dechlorination of g-hexachlorocyclohexane by zero-valent metallic iron, *J. Hazard. Mater.*, 2009, 166, 992-997.

4 M. C. Pereira, F. S. Coelho, C. C. Nascentes, J. D. Fabris, M. H. Araujo, K. Sapag, L. C. A. Oliveira and R. M. Lago, Use of activated carbon as a reactive support to produce highly active-regenerable Fe-based reduction system for environmental remediation, *Chemosphere*, 2010, 81, 7-12.

5 F. Magalhaes, M. C. Pereira, J. D. Fabris, S. E. C. Bottrel, M. T. C. Sansiviero, A. Amaya, N. Tancredi and R. M. Lago, Novel highly reactive and regenerable carbon/iron composites prepared from tar and hematite for the reduction of Cr(VI) contaminant, *J. Hazard. Mater.*, 2009, 165, 1016-1022.

6 F. D. Coelho, J. D. Ardisson, F. C. C. Moura, R. M. Lago, E. Murad and J. D. Fabris, Potential application of highly reactive Fe(0)/Fe_3O_4 composites for the reduction of Cr(VI) environmental contaminants, *Chemosphere*, 2008, 71, 90-96.

7 L. Z. Zhuang, Q. H. Li, J. S. Chen, B. B. Ma and S. X. Chen, Carbothermal preparation of porous carbon-encapsulated iron composite for the removal of trace hexavalent chromium, *Chem. Eng. J.*, 2014, 253, 24-33.

8 R. Yang, Y. Wang, M. Li and Y. J. Hong, A New Carbon/Ferrous Sulfide/Iron Composite Prepared by an *in Situ* Carbonization Reduction Method from Hemp (*Cannabis sativa L.*) Stems and Its Cr(VI) Removal Ability, *ACS Sustainable Chem. Eng.*, 2014, 2, 1270-1279.

9 C. C. Amorim, M. M. D. Leão, P. R. Dutra, J. C. Tristão, F. Magalhães and R. M. Lago, Use of tar pitch as a binding and reductant of BFD waste to produce reactive materials for environmental applications, *Chemosphere*, 2014, 109, 143-149.

10 R. F. Yu, F. H. Chi, W. P. Cheng and J. C. Chang, Application of pH, ORP, and DO monitoring to evaluate chromium(VI) removal from wastewater by the nanoscale zero-valent iron (nZVI) process, *Chem. Eng. J.*, 2014, 255, 568-576.

11 G. H. Lan, X. Hong, Q. Fan, B. Luo, P. Shi and X. L. Chen, Removal of Hexavalent Chromium in Wastewater by Polyacrylamide Modified Iron Oxide Nanoparticle, *J. Appl. Polym. Sci.*, 2014, *131*, 40945.

12 S. A. Baig, Q. Wang, Z. X. Wang, J. Zhu, Z. M. Lou, T. T. Sheng and X. H. Xu, Hexavalent Chromium Removal from Solutions: Surface Efficacy and Characterizations of Three Iron Containing Minerals, *Clean – Soil, Air, Water*, 2014, 42, 1409-1414.

13 S. Hanif and A. Shahzad, Removal of chromium(VI) and dye Alizarin Red S (ARS) using polymer-coated iron oxide (Fe_3O_4) magnetic nanoparticles by co-precipitation method, *J. Nanopart. Res.*, 2014, 16, 1-15.

14 A. R. Esfahani, S. Hojati, A. Azimi, L. Alidokht, A. Khataee and M. Farzadian, Reductive removal of hexavalent chromium from aqueous solution using sepiolite-stabilized zero-valent iron nanoparticles: Process optimization and kinetic studies, *Korean J. Chem. Eng.*, 2014, 31, 630-638.

15 X. Sun, Y. B. Yan, J. S. Li, W. Q. Han and L. J. Wang, SBA-15-incorporated nanoscale zero-valent iron particles for chromium(VI) removal from groundwater: mechanism, effect of pH, humic acid and sustained reactivity, *J. Hazard. Mater.*, 2014, 266, 26-33.

16 F. L. Fu, J. Ma, L. P. Xie, B. Tang, W. J. Han and S. Y. Lin, Chromium removal using resin supported nanoscale zero-valent iron, *J. Environ. Manage.*, 2013, 128, 822-827.

17 T. V. Toledo, C. R. Bellato, K. D. Pessoa and M. P. F. Fontes, Application of nanostructured iron oxides as adsorbents and photocatalysts for wastewater removal, *Quím. Nova*, 2013, 36, 419-425.

18 X. S. Lv, J. Xu, G. M. Jiang, J. Tang and X. H. Xu, Highly active nanoscale zero-valent iron (nZVI)–Fe_3O_4 nanocomposites for the removal of chromium(VI) from aqueous solutions, *J. Colloid Interf. Sc.*, 2012, 369, 460-469.

19 M. Barreto-Rodrigues, F. T. Silva and T. C. B. Paiva, Combined zero-valent iron and fenton processes for the treatment of Brazilian TNT industry wastewater, *J. Hazard. Mater.*, 2009, 165, 1224-1228.

20 R. C. C. Costa, F. C. C. Moura, P. E. F. Oliveira, F. Magalhães, J. D. Ardisson and R. M. Lago, Controlled reduction of red mud waste to produce active systems for environmental applications: heterogeneous Fenton

reaction and reduction of Cr(VI), *Chemosphere*, 2010, 78, 1116-1120.

21 A. Ghauch, Rapid removal of flutriafol in water by zero-valent iron powder, *Chemosphere*, 2008, 71, 816-826.

22 J. Li, Y. Li and Q. Meng, Removal of nitrate by zero-valent iron and pillared bentonite, *J. Hazard. Mater.*, 2010, 174, 188-193.

23 R. C. C. Costa, F. C. C. Moura, J. D. Ardisson, J. D. Fabris and R. M. Lago, Highly active heterogeneous Fenton-like systems based on Fe^0/Fe_3O_4 composites prepared by controlled reduction of iron oxides, *Appl. Catal. B-Environ.*, 2008, 83, 131-139.

24 F. C. C. Moura, M. H. Araujo, I. Dalmazio, T. M. A. Alves, L. S. Santos, M. N. Eberlin, R. Augusti and R. M. Lago, Investigation of reaction mechanisms by electrospray ionization mass spectrometry: characterization of intermediates in the degradation of phenol by a novel iron/magnetite/hydrogen peroxide heterogeneous oxidation system, *Rapid Commun. Mass Sp.*, 2006, 20, 1859-1863.

25 F. C. C. Moura, G. C. Oliveira, M. H. Araujo, J. D. Ardisson, W. A. A. Macedo and R. M. Lago, Highly reactive species formed by interface reaction between Fe^0–iron oxides particles: An efficient electron transfer system for environmental applications, *Appl. Catal. A-Gen.*, 2006, 307, 195-204.

26 C. C. Amorim, P. R. Dutra, M. M. D. Leao, M. C. Pereira, A. B. Henriques, J. D. Fabris and R. M. Lago, Controlled reduction of steel waste to produce active iron phases for environmental applications, *Chem. Eng. J.*, 2012, 209, 645-651.

27 P. E. F. Oliveira, L. D. Oliveira, J. D. Ardisson and R. M. Lago, Potential of modified iron-rich foundry waste for environmental applications: Fenton reaction and Cr(VI) reduction, *J. Hazard. Mater.*, 2011, 194, 393-398.

28 T. Ochi, S. Okubo and K. Fukui, Development of recycled PET fiber and its application as concrete-reinforcing fiber, *Cem. Concr. Compos.*, 2007, 29, 448-455.

29 C. T. Ferreira, J. B. da Fonseca and C. Saron, Recycling of Wastes from Poly(ethylene tereftalate) (PET) and Polyamide (PA) by Reactive Extrusion for Preparation of Polymeric Blends, *Polimeros-Ciencia e Tecnologia*, 2011, 21, 118-122.

30 A. F. Avila and M. V. Duarte, A mechanical analysis on recycled PET/HDPE composites, *Polym. Degrad. Stabil.*, 2003, 80, 373-382.

31 M. G. Rosmaninho, E. Jardim, G. L. Ferreira, M. H. Araujo, R. M. Lago and F. C. C. Moura, Partial hydrolysis of pet surface: transforming a plastic waste into a material with cationic exchange properties for environmental application, *Quím. Nova*, 2009, 32, 1673-1676.

32 O. Y. Marzouk, R. M. Dheilly and M. Queneudec, Valorization of post-consumer waste plastic in cementitious concrete composites, *Waste Manage.*, 2007, 27, 310-318.

33 C. Ingrao, A. Lo Giudice, C. Tricase, R. Rana, C. Mbohwa and V. Siracusa, Recycled-PET fibre based panels for building thermal insulation: environmental impact and improvement potential assessment for a greener production, *Sci. Total Environ*, 2014, 493, 914-929.

34 A. Esfandiari, T. Kaghazchi and M. Soleimani, Preparation and evaluation of activated carbons obtained by physical activation of polyethyleneterephthalate (PET) wastes, *J. Taiwan Inst. Chem. E.*, 2012, 43, 631-637.

35 E. Ali, K. Tahereh and S. Mansooreh, Preparation of high surface area activated carbon from Polyethylene terephthalate (PET) waste by physical activation, *Res J Chem Environ.*, 2011, 15, 433-437.

36 F. S. Zhang and H. Itoh, Use of specific gene analysis to assess the effectiveness of surfactant-enhanced trichloroethylene cometabolism, *J. Hazard. Mater.*, 2003, 101, 323-337.

37 A. P. C. Teixeira, J. C. Tristao, M. H. Araujo, L. C. A. Oliveira, F. C. C. Moura, J. D. Ardisson, C. C. Amorim and R. M. Lago, Iron: a versatile element to produce materials for environmental applications, *J. Braz. Chem. Soc.*, 2012, 23, 1579-1593.

38 D. Park, Y.-S. Yun and J. M. Park, XAS and XPS studies on chromium-binding groups of biomaterial during Cr(VI) biosorption, *J. Colloid Interf. Sci.*, 2008, 317, 54-61.

39 L. Joseph, L. K. Boateng, J. R. V. Flora, Y.-G. Park, A. Son, M. Badawy and Y. Yoon, Removal of bisphenol A and 17α-ethinylestradiol by combined coagulation and adsorption using carbon nanomaterials and powdered activated carbon, *Sep. Purif. Technol.*, 2013, 107, 37-47.

40 V. Gómez and M. P. Callao, Chromium determination and speciation since 2000, *TRAC-Trend Anal Chem.,* 2006, 25, 1006-1015.

41 Method 7196A - Chromium, Hexavalent (Colorimetric), http://www.caslab.com/EPA-Methods/PDF/EPA-Method-7196A.pdf).

42 I. Martin-Gullon, M. Esperanza and R. Font, Kinetic model for the pyrolysis and combustion of poly-(ethylene terephthalate) (PET), *J. Anal. Appl. Pyrol.*, 2001, 58, 635-650.

43 T. Shimada, T. Sugai, C. Fantini, M. Souza, L. G. Cancado, A. Jorio, M. A. Pimenta, R. Salto, A. Gruneis, G. Dresselhaus, M. S. Dresselhaus, Y. Ohno, T. Mizutani and H. Shinohara, Origin of the 2450 cm^{-1} Raman bands in HOPG, single-wall and double-wall carbon nanotubes, *Carbon*, 2005, 43, 1049-1054.

44 J. L. Figueiredo, M. F. R. Pereira, M. M. A. Freitas and J. J. M. Órfão, Modification of the surface chemistry of activated carbons, *Carbon*, 1999, 37, 1379-1389.

45 M. A. Aldosari, A. A. Othman and E. H. Alsharaeh, Synthesis and Characterization of the in Situ Bulk Polymerization of PMMA Containing Graphene Sheets

Using Microwave Irradiation, *Molecules*, 2013, 18, 3152-3167.